ELSEVIER

International Journal of Adhesion & Adhesives 27 (2007) 156–164

International Journal of Adhesion & Adhesives

www.elsevier.com/locate/ijadhadh

Enhancement of the adhesive joint strength of the epoxy–amine system via the addition of a resole-type phenolic resin

A. Sturiale, A. Vázquez, A. Cisilino, L.B. Manfredi*

Research Institute for Materials Science and Technology (INTEMA), Faculty of Engineering, National University of Mar del Plata—CONICET, Av. Juan B. Justo 4302 (7600) Mar del Plata, Argentina

Accepted 17 January 2006
Available online 19 May 2006

Abstract

In this paper the enhancement of the adhesive joint strength of the epoxy–amine system via the addition of a resole-type phenolic resin is investigated. Adhesive blends are formulated from a commercial epoxy and a synthesised resole-type phenolic resin. Phenolic contents are varied from 0% to 30%. The blends are characterized using Fourier transform infrared (FTIR) while the adhesive joint strength and the interfacial fracture toughness are studied for the adhesive blend/aluminium joint using single-lap shear and symmetrical and asymmetrical DCB specimens. It is found that the addition of resole improves the strength of the adhesive joint as well as its fracture toughness. The failure mode is found a function of the resole content. Resole contents less that 10% result in adhesive failure, while for resole contents of 20% and 30% the failure surfaces show adhesive and cohesive regions. The results allow concluding that the addition of resole-type phenolic resins constitutes an effective mean to enhance the adhesive properties of the epoxy–amine systems.

Keywords: Epoxy; Phenolic; Fracture mechanics; Mechanical properties of adhesives

1. Introduction

Epoxy resins are extensively used in the formulation of adhesives and protective coatings due to their excellent attributes such as chemical resistance, dielectric and insulation properties, low shrinkage on cure, dimensional stability and fatigue resistance [1]. The chemical compatibility of epoxy resins with a rather wide variety of polymers is also of great significance. A number of systems result from the blending of epoxy resins and polymeric modifiers such as nylon, phenolic resins and nitrile rubbers. The variety of chemical and mechanical properties that can be obtained from the combination of currently available epoxy resins and polymeric modifiers enables formulating epoxy-based adhesives and coatings to meet a wide range of specifications and usage criteria. The leading applications of the epoxy-based adhesives are in the field of structural metal bonding, particularly in the automotive and aerospace industry, in military equipment and in miscellaneous small-part assembly of plastics and metals. Phenolic modified epoxy resins produce one of the best high-temperature adhesives [2]. On the other hand, epoxy-based coatings are mainly used in plant maintenance, container coatings, appliance finishes, pipe coatings and trade sales paints. The most usual curing agents used for the formulation of epoxy-based coatings are amino compounds or formaldehyde condensates with phenols. The curing agents react with the hydroxyl groups of the epoxy backbone at elevated temperatures [1].

The final performance of multicomponent materials and structures depends significantly on the quality of the interface between its components. The need to improve the performance of multicomponent materials and structures has led to significantly progress in the area of interfacial fracture mechanics [3]. During the last few decades, a lot of works have been reported on the fracture of the metal/polymer interface. Most of them have been focused on the aluminium–epoxy interface [4–6].

Epoxy–phenolic systems have been used for many years in industrial applications, with formulations containing a variety of fillers and additives along with various types of

*Corresponding author. Fax: +54 223 4810046.
E-mail address: lbmanfre@fi.mdp.edu.ar (L.B. Manfredi).

0143-7496/$ - see front matter © 2006 Elsevier Ltd. All rights reserved.
doi:10.1016/j.ijadhadh.2006.01.007

epoxy prepolymers and curing agents. Each formulation can result in a resin which exhibits specific properties. To the authors' knowledge, there is no information about using the epoxy–amine–phenolic system as adhesive.

It is the aim of this work to characterise the epoxy–amine–phenolic systems and to evaluate the adhesive joint strength and the interfacial fracture toughness of the polymer blend/aluminium joint.

2. Interfacial fracture mechanics

A brief introduction to some interfacial fracture mechanics concepts is given in this section. This section does not pretend by any means to provide a detailed description of the phenomena, but to introduce the concepts and formulae used throughout the paper. For detailed information please refer to the work by Hutchinson and Suo [7].

2.1. Stress intensity factors and energy release rate for interface cracks

At the macroscopic level, the toughness of a joint may be characterized by the well-known remote stress intensity factors K_{I}^{∞} and K_{II}^{∞}. These stress intensity factors are determined from the applied loads and geometry, neglecting the presence of the adhesive layer (see Fig. 1(a)). On the other hand, when dealing at the microscopic level, the crack-tip stress fields may be regarded as being characterized by the complex stress intensity factor $\mathbf{K} = K_1 + \mathrm{i}K_2$. The real and imaginary components, K_1 and K_2, respectively, can be computed from Eq. (1) as follows:

$$K_1 = |\mathbf{K}|\cos(\widehat{\psi}),$$
$$K_2 = |\mathbf{K}|\sin(\widehat{\psi}), \tag{1}$$

where $\widehat{\psi}$ is the phase angle as depicted in Fig. 1(a). The phase angle $\widehat{\psi}$ characterizes the relative strength of the mode 2 to the mode 1 intensity factors acting on the interface crack at a reference (arbitrary) distance $\widehat{l}$ ahead the crack tip.

The phase angle is defined by

$$\widehat{\psi}(\widehat{l}) = \tan^{-1}\left(\frac{\mathrm{Im}(K\cdot\widehat{l}^{\,\mathrm{i}\varepsilon})}{\mathrm{Re}(K\cdot\widehat{l}^{\,\mathrm{i}\varepsilon})}\right), \tag{2}$$

where $\mathbf{K}$ is the complex stress intensity factor and ε the oscillatory index which depends on the elastic properties of the materials on both sides of the crack. Following Hutchinson and Suo [7] the reference distance $\widehat{l}$ was selected in this work based on a material length in order to facilitate the interpretation of mixed mode fracture data.

The above expressions are based on the assumption that the crack tip is open or, in other words, there is a direct transition from the band between the two materials to the free crack surfaces. However, Comninou [8] showed that the solution of the stress fields very close to the crack tip always predicts a contact zone between the crack surfaces at the crack tip. According to Rice [9] elastic fracture mechanics procedures (i.e. characterizing crack growth in terms of K) are still valid when the inevitable non-linear contact zone size, r_{c}, is small compared with the crack size, say $r_{\mathrm{c}}/\widehat{l} \ll 0.01$. An elementary estimation of the contact zone size is

$$\frac{r_{\mathrm{c}}}{\widehat{l}} = \exp\left[\frac{(\pi/2) - \widehat{\psi} + \tan^{-1}(2\varepsilon)}{\varepsilon}\right]. \tag{3}$$

Finally, the energy release rate for crack advance in the interface is

$$G = \frac{1}{\cosh^2(\pi\varepsilon)}\frac{|K|^2}{E^*}, \tag{4}$$

where E^* is the effective Young's modulus [7]. The criterion for initiation of crack advance in the interface when the crack tip is loaded in mixed mode characterized by $\widehat{\psi}$ is

$$G = \Gamma(\widehat{\psi}), \tag{5}$$

where the interface toughness, $\Gamma(\widehat{\psi})$, can be thought of as an effective surface energy that is a function of the mode of loading.

2.2. Crack paralleling an interface

A crack paralleling a bonded plane interface is considered in this section (see Fig. 1(b)). When the distance of the crack from the interface, δt, is small compared to the crack length itself and to other length scales characterizing the geometry, a simple universal relation exists between the remote stress intensity factors of the sub-interface crack, K_{I} and K_{II}, and the corresponding complex stress intensity factors of the interface crack, K_1 and K_2. This relation is independent of loading, crack length and external geometry [10]:

$$K_{\mathrm{I}} + \mathrm{i}K_{\mathrm{II}} = \sqrt{\frac{(1-\beta^2)}{(1+\alpha)}}\,\mathrm{e}^{\mathrm{i}\phi}(K)\,\delta t^{\mathrm{i}\varepsilon}, \tag{6}$$

where α and β are the so-called Dundur's parameters which are functions of the elastic properties of the materials on both sides of the crack. The symbol ϕ is a single dimensionless function of the elastic moduli that for sufficiently small α and β it can be approximated by [10]

$$\phi = 0.1584\alpha + 0.0630\beta. \tag{7}$$

Therefore, if the remote stress intensity factors are known, they can be immediately converted into the interface stress intensity factors with the universal relation (6). This observation provides the theoretical basis for developing sandwich specimens for measuring interface crack toughness.

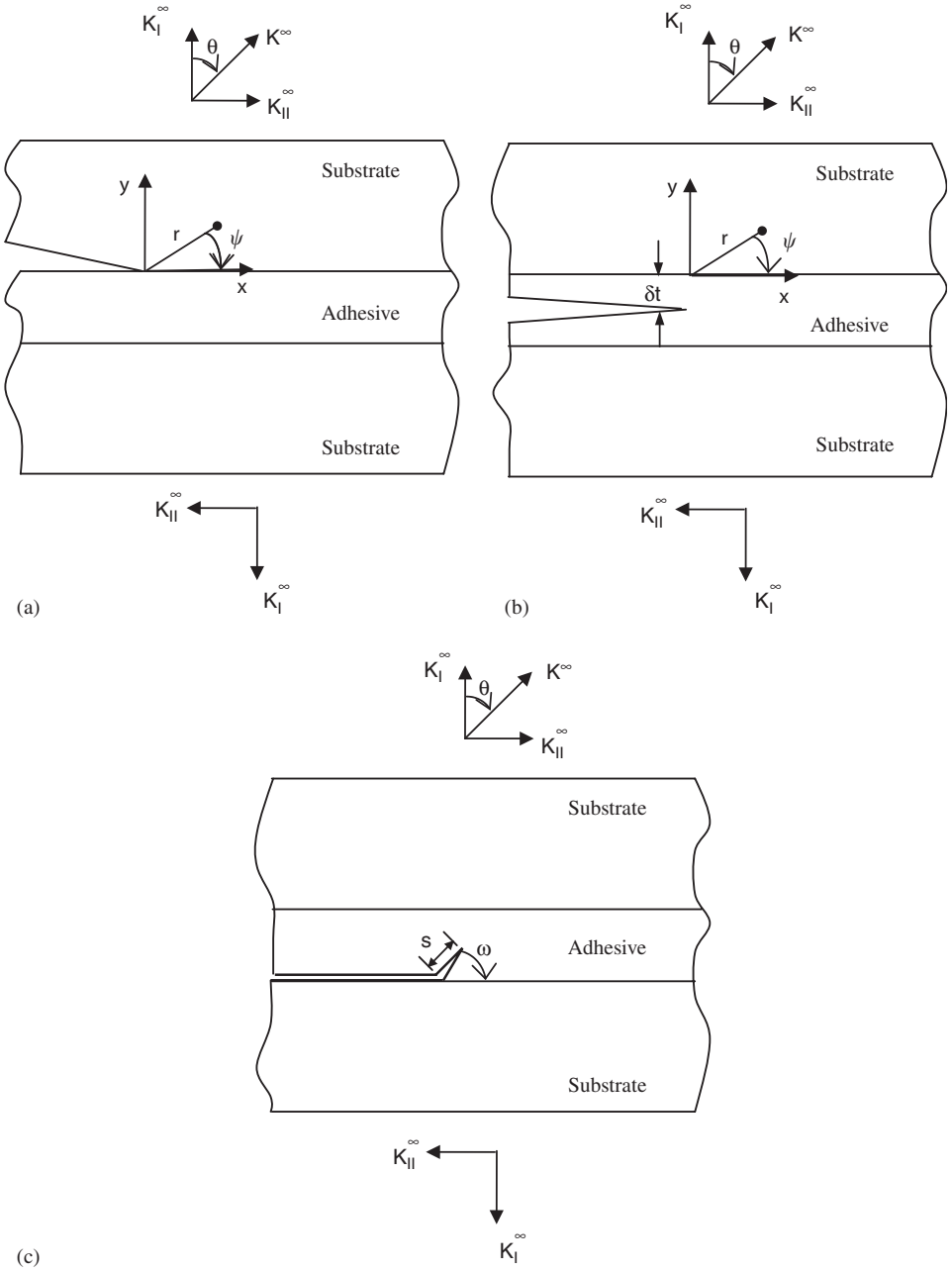

Fig. 1. (a) Crack on a bimaterial interface, (b) sub-interfacial crack and (c) interfacial crack with a kink-like flaw.

2.3. Kinking from an interface

Consider now an interfacial crack with a kink-like flaw of length s and orientation ω as illustrated in Fig. 1(c). A sufficient condition for the interfacial crack to kink out the interface of toughness $\Gamma_I(\widehat{\psi})$ into an adjacent material of toughness Γ_s is given by He and Hutchinson [11]

$$\frac{\Gamma_I(\widehat{\psi})}{\Gamma_s} \geqslant \frac{G_I}{G_s^*}, \tag{8}$$

where G_I is the energy release rate along the interface and G_s^* is the energy release rate at the tip of a kink such that $K_{II} = 0$. In order for the kink to grow away from the interface and across the layer, the stress intensity factors at the crack tip must satisfy the condition $K_I > 0$, $K_{II} \geqslant 0$. A kink with $K_{II} < 0$ is driven back towards the interface.

3. Experimental

3.1. Materials

The epoxy–amine–phenolic blends were formulated using an epoxy based on diglycidyl ether of bisphenol A (DGEBA GY250 from Ciba Geigy^{TM}) with epoxy equivalent of 189.8 g/mol. The amine triethylenetetramine technical grade (TETA, 70%, 34.5 g/equiv H) was utilized

as curing agent. The epoxy–amine system was used in stoichiometric ratio. Resole-type phenolic resin was synthesised with a formaldehyde to phenol molar ratio (F/Ph = 1.3) [12]. The adhesive blends were prepared using different phenolic contents: 0% (EA0), 10% (EA10), 20% (EA20) and 30% (EA30).

Test specimens were constructed using aluminium 6061 T6 as substrate (Young Modulus $E_1 = 69\,\text{GPa}$ and a Poisson ratio $\nu_1 = 0.33$). The aluminium surfaces at the interface sides were abraded using grid 180, 360 and 600 sandpapers and cleaned with acetone prior to the adhesive application. The curing profile was 15 min at 80 °C, 30 min at 130 °C and 15 min at 200 °C, at ambient preassure.

3.2. Methods

Fourier transform infrared (FTIR) analyses were performed using a Mattson Genesis 2 spectrometer with acquisition parameters as follows: 4000–400 cm^{-1} spectral width, 32 accumulations, and 2 cm^{-1} resolution.

A differential scanning calorimeter Shimadzu DSC-50 was used to determine the glass transition temperature of the blends. Tests were performed at 10 °C/min under nitrogen atmosphere.

An Instron 4467 machine was used for the mechanical tests (tensile, single-lap shear and mode I tests). All tests were performed at room temperature. The strength of the aluminium/adhesive joints were measured using Single Lap-Shear specimens following ASTM D-1002-94 [13]. Specimens were pin loaded using a controlled crosshead speed of 1.25 mm/min throughout the test. Five specimens were tested for each composition of the adhesive. The shape and dimensions of the specimens are depicted in Fig. 2(a). The adhesive was applied as a thin layer of 0.76 mm between the aluminium arms. The assemblies were joined and fastened between two glasses and the curing profile applied. Spacers were used to ensure the desired bond thickness.

Symmetrical double cantilever beam (DCB) specimens under remote mode I loading and asymmetrical double cantilever beam (ADCB) specimens under remote mixed mode loading were used for the determination of the aluminium/adhesive interfacial fracture toughness. The specimen dimensions are shown in Figs. 2(b) and (c). The adhesive layer was controlled by spacers placed at each end of the joint to ensure a $t = 0.8\,\text{mm}$ bond thickness. The mixed mode loading in the ADCB specimens was controlled by varying the relative heights of the aluminium arms. With this purpose the ratio of the top to the bottom height arms was set equal to 0.15. Initial cracks in the specimens were introduced along the bondlines by contaminating one of the metal surfaces with graphite powder and silicone release agent. Initial crack length was set $L =$ 30 mm for all specimens. All tests were performed using a constant displacement rate of 0.5 mm/min.

Stress intensity factors for the interface cracks were calculated by means of finite element analysis (FEA) and the universal relation (6) for sub-interface cracks. The procedure was as follows:

- record from the experiment the critical load for which the crack starts to propagate, P_{crit},
- construct a FEA model for the test specimen with a sub-interface crack of length L located at a (arbitrary) distance δt from the interface,
- use a FEA model to compute the mixed-mode stress intensity factors K_{I} and K_{II} for the sub-interface crack subjected to the remote load P_{crit},
- compute the complex stress intensity factors K_1 and K_2 for the interface crack using the K_{I} and K_{II} results and the universal relation given in Eq. (6).

FEA models were carried out using the Franc2D software [14], which includes the facility to compute mixed-mode stress intensity factors for cracks in homogeneous materials using the virtual crack extension method. A typical model discretization is depicted in Fig. 3. Three types of elements were employed in the model discretizations: eight-node quadrilateral elements in the zone away from the crack tip; quarter-point singular elements around the crack tip; and six-node triangular elements in the vicinity of the crack. Triangular elements serve to accommodate the transition in the mesh from the highly refined zone around the crack tip to the regular quadrilateral away from the crack tip. Preliminary tests allowed us to conclude that, for the proposed discretization scheme, the optimum distance δt for locating the sub-interface crack is in the range $0.10 < \delta t/t < 0.15$. Consequently a $\delta t = 0.12\,\text{mm}$ was adopted for all the models (see Fig. 1(b)). FEA results were validated by comparing with an analytical solution by Suo and Hutchinson [15] for DCB specimens and results with an error less than 1% were obtained. Plane strain conditions were assumed for all the finite element analysis and it was verified in every case that the adherents did not yield during the test.

4. Results and discussion

4.1. Characterization of the adhesives

Epoxy–amine–phenolic systems were characterised by means of FTIR. Fig. 4 shows the proposed reactions between epoxy and resole resin [16–18]. The presence of the compounds involving these reactions was followed in the FTIR spectra. The band at 1610 cm^{-1} which corresponds to the stretching of the aromatic ethylene bond [ν(C=C)] in the aromatic ring was taken as Ref. [19].

From the analysis of the products of the reactions (a) and (b) in Fig. 4, it can be argued that the content of ether groups, epoxy rings, hydroxyls of the phenols and methylols of the resole serve to study the progress of the reaction. In this way, an increment in the content of ether groups will follow the addition of resole to the epoxy resin,

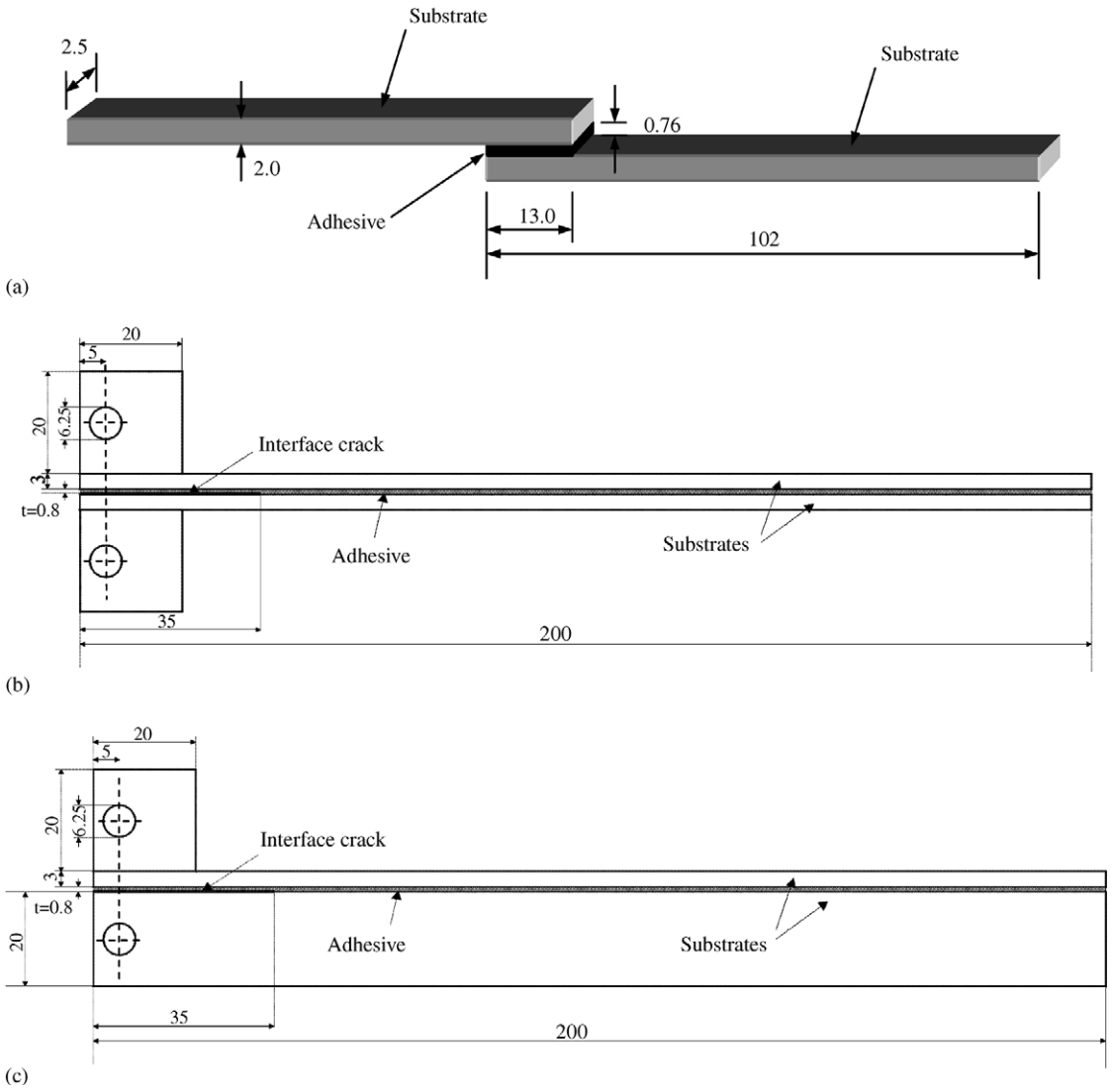

Fig. 2. Test specimens. Dimensions (in mm) of the (a) Single Lap-Shear, (b) symmetrical double cantilever beam and (c) asymmetrical double cantilever beam specimens.

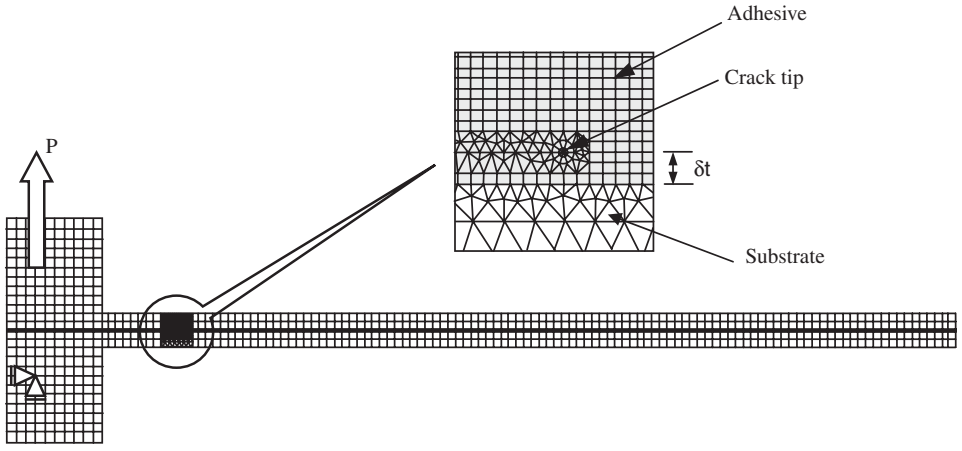

Fig. 3. Finite element discretization strategy for the computation of stress intensity factors.

while the content of epoxy rings, hydroxyls of the phenols and methylols of the resoles should decrease accordingly. On the other hand, the secondary hydroxyls of the epoxy cannot be used to study the reaction progress, as they are consumed and produced during the reactions. Figs. 5 and 6 show the FTIR spectra of the resole, epoxy–amine and

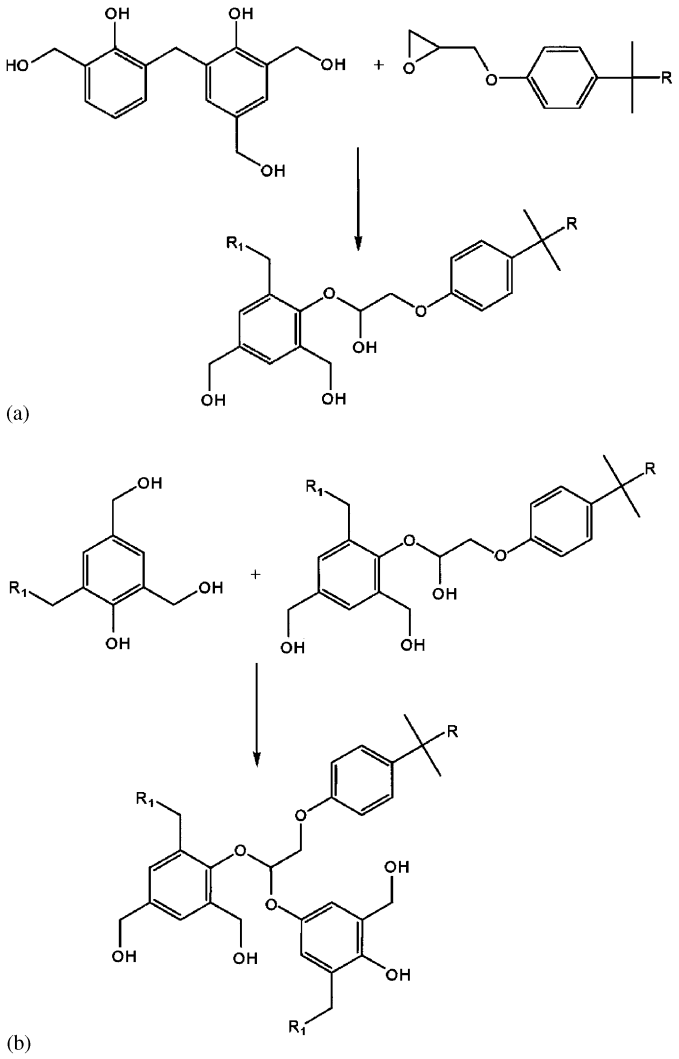

Fig. 4. Proposed reactions between the epoxy and resole resin.

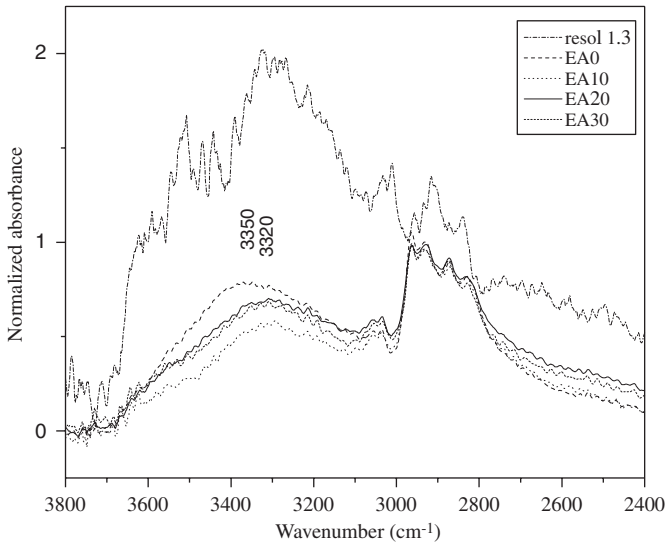

Fig. 5. FTIR spectra of epoxy–amine–phenolic blends in the 3800–2400 cm^{-1} spectral width.

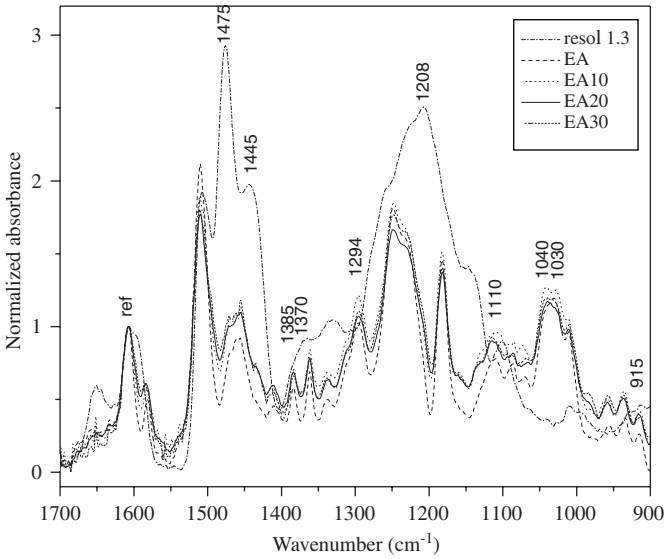

Fig. 6. FTIR spectra of epoxy–amine–phenolic blends in the 1700–900 cm^{-1} spectral width.

their blends in the 3800–2400 cm^{-1} range and 1700–900 cm^{-1} range, respectively.

The bands at 1294 cm^{-1} [ν (CO)], 1110 cm^{-1} [ν (COC)] and 1040 cm^{-1} [ν (φOC)] are characteristic of the ether group [20–22], where φ is the benzene ring. It was observed that these bands became higher with the addition of resole to the epoxy–amine system.

A decrease in the content of phenols hydroxyl and methylols of the resole was observed in the spectra of the blends in the band from 3600 to 3200 cm^{-1}. This is the characteristic region of the OH groups [21,23,24]. These hydroxyls groups react with the epoxy resin to form ether groups (see Fig. 4). In addition, the bands at 1370 and 1208 cm^{-1} that correspond to the formation of the OH [δ (OH)] and ν (CO) of the phenol, respectively [21,23,24], appear in the spectrum of the resole but they are not present in the spectra of the blends. So, indicating that a reaction exists between the phenol and the epoxy resins.

The band at 915 cm^{-1} that corresponds to the epoxy ring [20–22] is overlapped with the band of the $\delta(\varphi$–$H)$ of the substituted benzene ring of the phenolic resin, so, it can not be used to study the reactions.

The methylene bridges of the resole are identified by the bands at 1475 and 1445 cm^{-1} [23,24]. These bands are smaller for the epoxy–amine and the blends than for the resole resin. This indicates that during the crosslinking reaction of the phenolic resin the formation of the bridges is easier when the resole is alone than in the presence of the epoxy–amine system. So, from the FTIR spectra of the blends it was possible to conclude that the epoxy reacts with the resole resin.

The glass transition temperature and the Young modulus were measured for all the blends. The Tg values obtained using DSC are given in the Table 1. The Young moduli of the blends were measured from tensile tests and following ASTM D 638M-93 [25]. The results are shown in

Table 1
Glass transition temperature as a function of the resole content

Adhesive	T_g (°C)
EA0	111
EA10	100
EA20	102

Table 2
Tensile moduli of the adhesive blends as a function of the resole content

Adhesive	E_1 (GPa)
EA0	4.30
EA10	3.75
EA20	2.85
EA30	2.45

Table 3
Dundur's parameters, α and β, oscillatory index, ε, and function ϕ for the aluminium/adhesive bimaterials

Adhesive	EA0	EA10	EA20	EA30
α	0.88096	0.89539	0.91949	0.93039
β	0.20193	0.20543	0.21127	0.21391
ε	−0.06517	−0.06633	−0.06828	−0.06916
ϕ	0.15227	0.15477	0.15896	0.16085

Table 2. It can be observed that the modulus diminishes with the increment in the phenolic content. On the other hand, the Poisson ratio was estimated $v_2 = 0.35$ for all the blends from the data available in the bibliography [4,6]. Values of the Dundur's parameters α and β, the oscillatory index ε and the function ϕ for the resulting aluminium/adhesive bimaterials are given in Table 3. These results will be used later in the determination of the interfacial fracture toughness of the blends.

4.2. Adhesive joint strength

The Single Lap-Shear test was used to evaluate the strength of the adhesive joints. Fig. 7 shows the average shear stress obtained for the different adhesives. It can be observed that the addition of resole to the epoxy–amine system improves the strength of the adhesive joint from 4 to 8.50 MPa. Error bars indicate the dispersion of the results. Also included as a reference in Fig. 7 is the value reported by Gordon and Fakley [26] for an epoxy adhesive without the addition of resole. Obtained results for the EA0 adhesive are in excellent agreement with that of the reference.

Examination of the post-mortem fractured surfaces revealed that the failure mode of the specimens is a function of the phenolic percentage in the adhesive. For resole contents lower than or equal to 10% (adhesives EA0 and EA10) the failure was adhesive. On the other hand, the crack surfaces showed adhesive and cohesive regions for the formulations EA20 and EA30, with the crack growing along both the interface and the bulk.

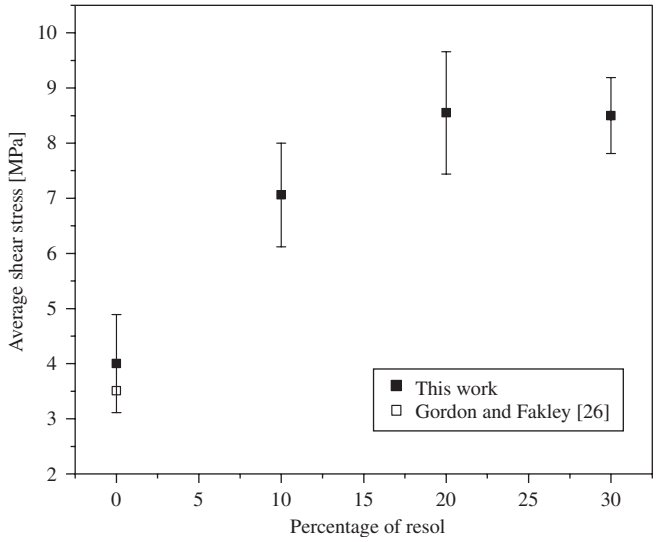

Fig. 7. Results of the Single Lap-Shear test as a function of the resole content.

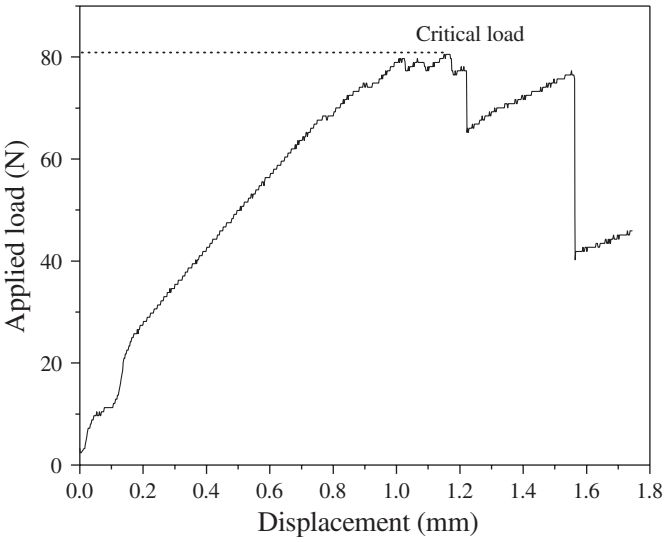

Fig. 8. Typical load vs. displacement record for DCB specimen.

4.3. Interfacial fracture toughness

The fracture toughness of the adhesive–metal interface cracks was assessed using DCB and ADCB specimens and the procedure introduced in Section 3.2. Fig. 8 depicts a typical load vs. displacement record for DCB specimen, where the critical load, $P_{crit.}$, corresponds to the onset of crack propagation.

4.3.1. Symmetric DCB specimens

The critical loads for the symmetrical DCB specimens are reported in Table 4. Results are presented in terms of

Table 4
Critical loads for the symmetrical DCB specimens

Adhesive	P_{crit} (N)
EA0	21.0±12.7
EA10	58.6±24.9
EA20	71.9±18.2
EA30	86±10.8

Table 5
K_1, K_2, $\widehat{\psi}$ and $\Gamma(\widehat{\psi})$ values for the interface cracks in the DCB specimens

Adhesive	EA0	EA10	EA20	EA30
K_1 (MPa $\sqrt{\text{mm}}$)	7.31	19.05	20.75	23.27
K_2 (MPa $\sqrt{\text{mm}}$)	3.03	−8.11	−9.06	−10.27
$\widehat{\psi}$ (*deg*)	−13.93	−14.30	−14.57	−14.95
$\Gamma(\widehat{\psi})$ (J/m^2)	6.51	50.66	78.55	114.56

the mean values and the correspondent standard deviations resulting from the analysis of the test data. It can be observed that the addition of resole to the epoxy–amine system results in an increment of the critical load. The major relative increment in the critical load occurs with resole contents up to 20%.

Following the procedure introduced in Section 3.2, the interface stress intensity factors K_1 and K_2 were calculated by means of the universal relation (6) and the mixed-mode stress intensity factors computed using FEA models for cracks paralleling the bonded plane. The resulting values are reported in Table 5. Also included in Table 5 are the interface fracture toughness $\Gamma(\widehat{\psi})$ results which were computed using Eqs. (4) and (5). The characteristic length used throughout the calculations was arbitrarily chosen $l = 100\,\text{mm}$. It is worth to note that the results in Table 5 were computed using the mean values of the critical loads given in Table 4.

The validity of the reported K results was assessed by checking the extent of the crack tip contact zone using expression (3). The resulting value $r_c/\widehat{l} \cong 3 \times 10^{-11} \ll 0.01$ clearly secured the occurrence of a small enough contact zone between the crack surfaces at the crack tip. The phase angles for all the specimens were in the range $14^\circ \leqslant \widehat{\psi} \leqslant 15^\circ$.

The above results show that the interfacial fracture energy presents important improvement with the amount of phenolic resin added to the adhesives. At the same time it is found that the interfacial fracture toughness obtained for the epoxy adhesive (EA0) is comparable with results available in the literature. Thus, Charalambides et al. [27] reported $\Gamma = 12.3\,\text{J/m}^2$ for the PMMA/Al adhesive interface while Akisanya et al. [4] reported $\Gamma = 20\,\text{J/m}^2$ for epoxy/Al.

The analysis of the fracture surfaces showed that with the only exception of specimens assembled using the EA0 adhesive, all the samples presented an alternating crack path. This path is due to the periodic kinking of the interfacial crack whereby the crack departs from one interface and grows across the adhesive layer until it becomes an interfacial crack on the opposing interface. This observation is in agreement with the behaviour reported for the Lap-Shear tests (see Section 4.2). The crack kinks away from the interface when the interfacial phase angle at the crack tip attains a critical value, in accordance with the condition presented in Eq. (8).

The minimum value for the adhesive fracture toughness necessary for preventing the crack to propagate away from the interface was calculated using a FEM model for the EA20 adhesive. With this purpose a finite element model of a kinked interface crack similar to that depicted in Fig. 1c was constructed. The length $s = 0.4\,\text{mm}$ and the orientation $\omega = 30^\circ$ were selected for the kink. Stress intensity factors for the interface crack, $K_1 = 24.17\,\text{MPa}\sqrt{\text{mm}}$ and $K_2 = 2.27\,\text{MPa}\sqrt{\text{mm}}$, were computed following the procedure outlined in Section 2.2. On the other hand, the stress intensity factors for the kink crack, $K_I = 18.29\,\text{MPa}\sqrt{\text{mm}}$ and $K_{II} = -1.23\,\text{MPa}\sqrt{\text{mm}}$, were directly computed by Franc2D/L as the crack tip is surrounded by a homogeneous material. Although the mode II stress intensity factor of the kink crack does not strictly fulfill the condition $K_{II} = 0$, it was considered low enough with respect to K_I ($K_{II} < 0.07\ K_I$) to check the condition in Eq. (8).

The energy release rate along the interface $G_I = 51.50\,\text{J/m}^2$ was computed using Eq. (4), while the energy release rate at the tip of the kink is $G_s^* = K_I^2/E_2 = 117.38\,\text{J/m}^2$. Then, from Eq. (8) it follows

$$\Gamma_s \leqslant \frac{\Gamma\left(\widehat{\psi}\right) G_s^*}{G_I} = \frac{78.55\,(\text{J/m}^2) \times 117.38\,(\text{J/m}^2)}{51.50\,(\text{J/m}^2)} = 172.95\,\text{J/m}^2. \quad (9)$$

Considering that the fracture toughness of the epoxy $\Gamma = 50\,\text{J/m}^2$ [4] and that the addition of resole reduces this value, the above result clearly predicts the occurrence of an alternating crack path. Also in accordance with the above result is the load vs. deflection response illustrated in Fig. 8, which depicts an ''alternating'' trace after the maximum load is attained. This behaviour is in accordance with the results reported by Akisanya et al. [4] for alternating cracks.

4.3.2. Asymmetric DCB specimens

Only the EA20 adhesive joint (the adhesive with the highest joint strength, see Section 4.2) was tested using the ADCB configuration. The mean value and standard deviation for the critical load result were $P_{crit.} = 127 \pm 16.2\,\text{N}$.

The interfacial stress intensity factors were computed following the same procedure employed for the symmetric specimen, resulting in the values reported in Table 6. Also reported in Table 6 is the interfacial toughness $\Gamma(\widehat{\psi}) = 213.62\,\text{J/m}^2$, which was computed using expressions

Table 6
$K1$, $K2$, $\widehat{\psi}$ and $\Gamma(\widehat{\psi})$ for the interface crack in the ADCB specimen

Adhesive	EA20
K_1 $(\text{MPa}\sqrt{\text{mm}})$	24.57
K_2 $(\text{MPa}\sqrt{\text{mm}})$	−28.11
$\widehat{\psi}$ (deg)	−39.84
$\Gamma(\widehat{\psi})$ (J/m^2)	213.62

(4) and (5) for the mean critical load. The phase angle for the characteristic length $\widehat{l} = 100\,\text{mm}$ was $\widehat{\psi} = -39.48^\circ$. The increment in the interfacial fracture toughness with the mixed mode conditions is similar to that reported by Akisanya et al. [4] for the epoxy/Al joint.

5. Conclusions

The formulation and mechanical characterization of adhesives based on epoxy–amine–phenolic blends have been presented in this work. The adhesive blends were formulated from a commercial epoxy and a synthesised resole-type phenolic resin with phenolic contents ranging from 0% to 30%. FTIR analyses allowed concluding that the epoxy reacts with the phenolic resin. The Young moduli of the blends diminished with the increment in the phenolic content, from 4.30 MPa for 0% resole to 2.45 GPa for a resole content of 30%.

The strength and the interfacial fracture toughness were investigated for the adhesive-aluminium interface. It was found that the addition of resole improves both, the adhesive joint strength and the interfacial fracture toughness. The major relative improvements in both cases were achieved with resole contents in the range from 10% to 20%.

The failure mode was found a function of the resole content. For a resole contents lower than 10% the failure was adhesive, while for resole contents of 20% and 30% the crack surfaces showed adhesive and cohesive regions. The conditions for the occurrence of the alternating crack path were confirmed by means of FEA results and fracture mechanics analysis.

The above reported results allow concluding that the addition of resole-type phenolic resins constitutes an effective mean to enhance the adhesive properties of the epoxy–amine systems.

Acknowledgements

The authors appreciate the financial support provided by Consejo Nacional de Investigaciones Científicas y Técnicas (CONICET) and the Agencia Nacional de Promoción Científica y Tecnológica (ANPCYT) of the República Argentina under grants PICT 12-12528 and 12-14600.

References

[1] Paul S. In: Paul S, editor. Surface coatings. 2nd ed. New York: Wiley; 1996. p. 243, 246 and 264.
[2] Lewis AJ. In: May CA, editor. Epoxy resins: chemistry and technology. 2nd ed. New York: Marcel Dekker Inc.; 1988. p. 655 and 711.
[3] Schultz J, Nardin M. In: Pizzi A, Mittal KL, editors. Handbook of adhesive technology. New York: Marcel Dekker Inc.; 1994.
[4] Akisanya AR, Fleck NA. Int J Fract 1992;58:93.
[5] Ikeda T, Miyazaki N, Soda T. Eng Fract Mech 1998;59(6):725.
[6] Chen B, Dillard DA. Int J Solids Struct 2001;38:6907.
[7] Hutchinson JW, Suo Z. Adv Appl Mech 1992;29:63.
[8] Comninou M. ASME J Appl Mech 1977;44:631.
[9] Rice JR. ASME J Appl Mech 1988;55:98.
[10] Hutchinson JW, Mear ME, Rice JR. ASME J Appl Mech 1987;54:828.
[11] He MY, Hutchinson JW. Int J Solids Struct 1989;25(9):1053.
[12] Manfredi LB, de la Osa O, Galego Fernandez N, Vázquez A. Polymer 1999;40(13):3867.
[13] ASTM D-1002-94. Standard Test Method for Apparent Shear Strength of Single-Lap-Joint Adhesively Bonded Metal Specimens by Tension Loading.
[14] Wawrzynek P, Ingraffea A. FRANC2D, Cornell Fracture Group, University of Cornell, USA; 1993.
[15] Suo Z, Hutchinson JW. Mater Sci Eng 1989;A107:135.
[16] Mika TF, Bauer RS. In: May CA, editor. Epoxy resins: chemistry and technology. 2nd ed. New York: Marcel Dekker Inc.; 1988. p. 481.
[17] McAdams LV, Gannon JA, Ciba-Geigy Corporation. In: Mark H, Bikales N, Overberger C, Menges G, Kroschwitz J, editors. Encyclopedia of polymer science and engineering. 2nd ed. vol. 6. New York: Wiley; 1985. p. 322.
[18] Ashcroft WR. In: Ellis B, editor. Chemistry and technology of epoxy resins. 1st ed. Great Britain: Chapman & Hall; 1993. p. 66.
[19] Rockniak C, Biernacka T, Skarzynski M. J Appl Polym Sci 1983;28:531.
[20] Mertzel E, Koenig JL. Adv Polym Sci 1986;75:74.
[21] Lin-Vien D, Colthup NB, Fateley WG, Grasselli JG. The handbook of infrared and Raman characteristic frequencies of organic molecules. London: Academic Press; 1991.
[22] Lin SC, Bulkin BJ, Pearce EM. J Appl Polym Sci 1979;17:3121.
[23] Holopainen T, Alvila L, Rainio J, Pakkanen TJ. Appl Polym Sci 1998;69:2175.
[24] Grenier-Loustalot MF, Larroque S, Grenier P. Polymer 1996;37(4): 639.
[25] ASTM D 638M-93. Test method for tensile properties of plastics.
[26] Gordon TL, Fakley ME. Int J Adhesion Adhesives 2003;23:95.
[27] Charalambides PG, Lund J, Evans AG, McMeeking RM. J Appl Mech 1989;56:77.